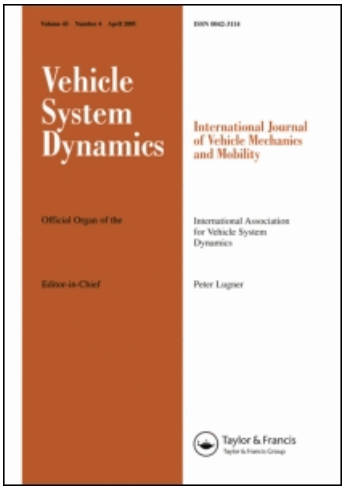

Vehicle System Dynamics
Publication details, including instructions for authors and subscription information:
http://www.informaworld.com/smpp/title~content=t713659010

Lateral load transfer and normal forces estimation for vehicle safety: experimental test

M. Doumiati [a]; A. Victorino [a]; A. Charara [a]; D. Lechner [b]
[a] HEUDIASYC Laboratory, UMR CNRS 6599, Centre de recherche Royallieu, Université de Technologie de Compiègne, Compiègne, France [b] INRETS-MA Laboratory Department of Accident Mechanism Analysis, Chemin de la Croix Blanche, Salon de Provence, France

To cite this Article Doumiati, M., Victorino, A., Charara, A. and Lechner, D.(2009) 'Lateral load transfer and normal forces estimation for vehicle safety: experimental test', Vehicle System Dynamics, 47: 12, 1511 — 1533
To link to this Article: DOI: 10.1080/00423110802673091
URL: http://dx.doi.org/10.1080/00423110802673091

Vehicle System Dynamics
Vol. 47, No. 12, December 2009, 1511–1533

Taylor & Francis
Taylor & Francis Group

Lateral load transfer and normal forces estimation for vehicle safety: experimental test

M. Doumiati[a]*, A. Victorino[a], A. Charara[a] and D. Lechner[b]

[a]*HEUDIASYC Laboratory, UMR CNRS 6599, Centre de recherche Royallieu, Université de Technologie de Compiègne, BP 20529, 6200, Compiègne, France;* [b]*INRETS-MA Laboratory Department of Accident Mechanism Analysis, Chemin de la Croix Blanche, Salon de Provence, France*

(*Received 2 May 2008; final version received 3 December 2008*)

Knowledge of vehicle dynamics data is important for vehicle control systems that aim to enhance vehicle handling and passenger safety. This study introduces observers that estimate lateral load transfer and wheel–ground contact normal forces, commonly known as vertical forces. The proposed method is based on the dynamic response of a vehicle instrumented with cheap and currently available standard sensors. The estimation process is separated into three blocks: the first block serves to identify the vehicle's mass, the second block contains a linear observer whose main role is to estimate the roll angle and the one-side lateral transfer load, while in the third block we compare linear and nonlinear models for the estimation of four wheel vertical forces. The different observers are based on a prediction/estimation filter. The performance of this concept is tested and compared with real experimental data acquired using the INRETS-MA (Institut National de Recherche sur les Transports et leur Sécurité – Département Mécanismes d'Accidents) Laboratory car. Experimental results demonstrate the ability of this approach to provide accurate estimation, thus showing its potential as a practical low-cost solution for calculating normal forces.

Keywords: vehicle dynamics; state observers; load transfer; vertical tyre force estimation; rollover avoidance

1. Introduction

Extensive research has shown that over 90% of road accidents occur as a result of driver error [1]. Most drivers have little knowledge of dynamics, and so driver assistance systems have an important role to play. This is why the last few years have seen the emergence of on-board advanced driver assistance systems control systems in cars as a way of improving security and helping to prevent dangerous situations. Among these controllers we find systems such as the anti-lock braking system and electronic stability programs. Improving vehicle stabilisation and control decisions is possible when certain vehicle parameters, such as velocity, roll angle, yaw rate, sideslip angle, weight of the vehicle and wheel ground forces are known. Unfortunately, for technical, physical and economic reasons, some of these parameters are not measurable in a standard vehicle. For example, in [2,3] observers were proposed for estimating sideslip

*Corresponding author. Email: mdoumiat@hds.utc.fr

ISSN 0042-3114 print/ISSN 1744-5159 online

DOI: 10.1080/00423110802673091
http://www.informaworld.com

angle and lateral tyre force. Measuring tyre forces requires wheel transducers that currently cost in the region of €100,000, for a six-component measurement system, which is prohibitive for ordinary cars, and therefore this data must be observed or estimated. Knowledge of wheel–ground contact normal forces is essential for improving transport security. Vertical load on the tyre has a primary influence on steering behaviour, vehicle stability and cornering stiffness, which in turn determines the lateral force. Moreover, on-line measurement of vehicle tyre forces in a moving vehicle allows a better calculation of the road damage or lateral transfer ratio (LTR) parameter. LTR is an indicator used to prevent or forecast rollover situations [4]. The LTR coefficient is defined as the ratio of the difference between the sum of the left wheel loads and the right wheel loads to the sum of all the wheel loads. Estimating the vertical tyre load is generally considered a difficult task. Variations in the vehicle's mass, the position of the centre of gravity (cog), road grade, road irregularities and in load transfer increase the complexity of the problem.

In the literature, many studies have looked at the calculation of the wheel–ground contact normal forces. In [5], the author presents a model for calculating vertical forces. Lechner's model respects the superposition principle, assuming independent longitudinal and lateral acceleration contributions. In [6], a study of a 14 DOF (degree of freedom) vehicle model is proposed where the dynamics of the roll centre are used to calculate vertical tyre forces. In [7], the tyre forces are modelled by coupling longitudinal and lateral acceleration. Authors in [8] investigated the application of the dual extended Kalman filter for estimating vertical forces. They concluded that the obtained results differ from the reference data, the discrepancy being attributable to the problem of the vehicle's mass.

In this article, our main objective is to develop a real-time process for estimating the wheel–ground contact vertical forces, regardless of tyre model, while taking into account the constraints of industrial applicability. To simplify the model, pitch angle, road angle and

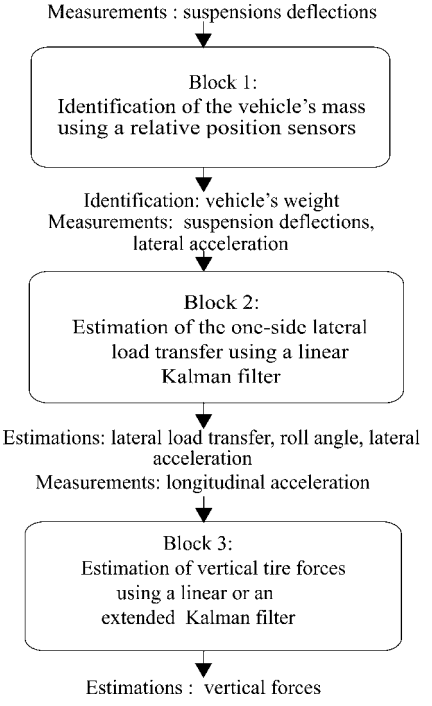

Figure 1. Description of the three-block estimation process.

road irregularities are not considered in our study. The proposed estimation process is modelled in three blocks as shown in Figure 1. The first block identifies the vehicle's mass at rest and calculates the static load applied to the vehicle. The identified mass will be used as a known vehicle parameter in the other blocks. The aim of the second block is to calculate the one-side lateral load transfer using roll dynamics. The estimated value will be considered as an essential measure for the third block, guaranteeing its convergency and observability. The third block estimates the four vertical tyre forces, and serves to calculate the LTR coefficient. Each block will be described in detail in the following sections. By using cascaded observers, the observability problems entailed by an inappropriate use of the complete modelling equations are avoided, enabling the estimation process to be carried out in a simple and practical way.

The structure of the article is organised as follows. Section 2 describes a method for identifying vehicle mass. In Sections 3 and 4, we describe in detail each of the observers designed for estimation of lateral load transfer and normal forces. Section 5 presents the method of estimation and the Kalman filter algorithm. Section 6 presents an observability analysis. Section 7 introduces the importance of vertical forces for rollover calculations. Section 8 presents briefly the road angle effects on normal forces. In Section 9, observer results are compared with experimental data, and then in the final section we make some concluding remarks regarding our study and future perspectives.

2. Block 1: identification of the vehicle's mass

The vehicle's mass is an important parameter in studying lateral load transfer and normal tyre forces. Moreover, knowing the load distribution when the vehicle is at rest is essential for initialising the observers (see Section 4). This section deals with this problem and presents a simple method for determining a vehicle's mass.

Determining the mass of a vehicle is a problem seldom discussed in the literature. For example, in [9], a recursive least-squares method is developed for online estimation of a vehicle's mass. This method cannot be effective in our application because it takes a considerable time to converge to the real mass value. The objective of this section is to identify the vehicle's mass, *at rest*, by considering a quarter-car model (Figure 2) and applying relative position sensors. Nowadays, many controlled suspensions are equipped with relative position sensors for measuring suspension deflections δ_{ij} (relative positions of the wheels z_2 with respect to the body z_1) at each corner, where i represents front (f) or rear (r) and j represents left (l) or right (r). The suspension spring is loaded with the corresponding sprung mass. The quarter mass m_{eij} (sum of the sprung and unsprung masses) at each corner of the empty vehicle is provided by the manufacturer. Given a conventional suspension without level regulation and assuming that it works in its linear range, and neglecting the tyre deflection, a load variation in the sprung mass Δm_{sij} changes the spring deflection $\delta_{ij} \rightarrow \delta_{ij} + \Delta ij$, where

$$\Delta m_{\mathrm{s}ij} = \frac{k_{\mathrm{s}} \Delta_{ij}}{g}; \tag{1}$$

Δ_{ij} is the spring deflection variation, k_s the spring stiffness and g the gravitational constant. The total quarter mass m_{ij} and the total mass of the vehicle m_{v} are then calculated as follows:

$$\begin{cases} m_{ij} = m_{eij} + \Delta m_{\mathrm{s}ij} \\ m_{\mathrm{v}} = \sum_{i,j} m_{ij}. \end{cases} \tag{2}$$

Then the static load (when the vehicle is at rest) applied to each wheel is equal to $m_{ij}g$. Experimental tests that validate the presented identification method are presented in Section 9.

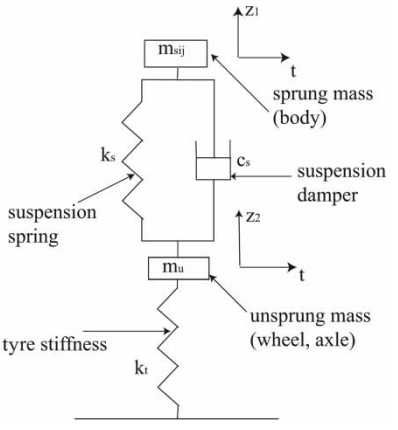

Figure 2. A quarter-car model with linear suspension.

In the remainder, the identified m_{ij} will be used in initialising observers (Section 4) and m_{v} as a known vehicle parameter.

3. Block 2: lateral transfer load model

The lateral load transfer model we have developed is based on the vehicle's roll dynamics. This dynamic considers a roll plane model including the roll angle θ, as shown in Figure 3. This model has a roll DOF for the suspension that connects the sprung and unsprung mass, and its sprung mass is assumed to rotate about the roll centre. During cornering, roll angle depends on the roll stiffness of the axle and on the position of the roll centre. The roll centre, which is defined as a point at which lateral forces applied to the sprung mass do not produce suspension roll, can be constructed from the lateral motion of the wheel contact points [10]. In reality, the roll centre of the vehicle does not remain constant, but in this study a stationary roll centre is assumed in order to simplify the model. The roll axis is defined as the line that passes through the roll centre at the front and rear axles (see Figure 4).

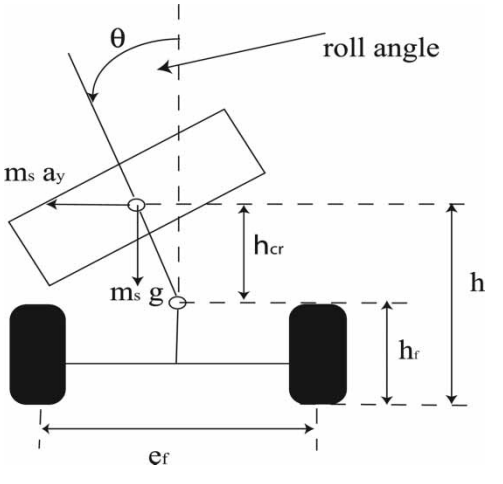

Figure 3. Roll dynamics.

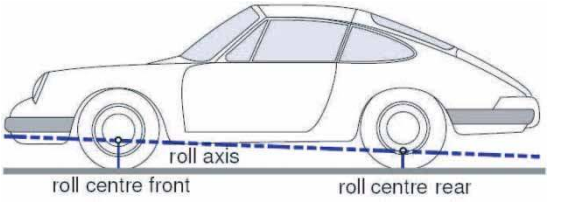

Figure 4. Roll axis.

According to the torque balance in the roll axis, the roll dynamics of the vehicle body can be described by the following differential equation (case of small roll angle):

$$I_{xx}\ddot{\theta} + C_{\mathrm{R}}\dot{\theta} + K_{\mathrm{R}}\theta = m_{\mathrm{s}}a_y h_{\mathrm{cr}} + m_{\mathrm{s}}h_{\mathrm{cr}}g\theta, \tag{3}$$

where I_{xx} is the moment of inertia of the sprung mass with respect to the roll axis, C_{R} and K_{R} denote, respectively, the total damping and spring coefficients of the roll motion of the vehicle's system, a_y is the lateral acceleration and h_{cr} the height of the sprung mass about the roll axis.

Summing the moments about the front and rear roll centres, the simplified steady-state equation for the lateral load transfer applied to the left part of the vehicle is given by the dynamic relationship (4):

$$\begin{aligned}\Delta Fz_l &= (Fz_{\mathrm{fl}} + Fz_{\mathrm{rl}} - Fz_{\mathrm{fr}} - Fz_{\mathrm{rr}}) \\ &= -2\left(\frac{k_{\mathrm{f}}}{e_{\mathrm{f}}} + \frac{k_{\mathrm{r}}}{e_{\mathrm{r}}}\right)\theta - 2m_{\mathrm{s}}\frac{a_y}{l}\left(\frac{l_{\mathrm{r}}h_{\mathrm{f}}}{e_{\mathrm{f}}} + \frac{l_{\mathrm{f}}h_{\mathrm{r}}}{e_{\mathrm{r}}}\right),\end{aligned} \tag{4}$$

where h is the height of the centre of gravity; h_{f} and h_{r} are the heights of the front and rear roll centres; e_{f} and e_{r} the front and rear vehicle's track, respectively; k_{f} and k_{r} the front and rear roll stiffnesses, respectively; l_{r} and l_{f} the distances from the cog to the front and rear axles, respectively; and l is the wheelbase ($l = l_{\mathrm{r}} + l_{\mathrm{f}}$) [10,11]. We note that the lateral load transfer in Equation (4) can be expressed with the following terms:

- $\Delta Fz_{\mathrm{ge}} = m_{\mathrm{s}}a_y/l(l_{\mathrm{r}}h_{\mathrm{f}}/e_{\mathrm{f}} + l_{\mathrm{f}}h_{\mathrm{r}}e_{\mathrm{r}})$ is the geometric load transfer, which depends on the height of the roll centres;
- $\Delta Fz_{\mathrm{el}} = \theta(k_{\mathrm{f}}/e_{\mathrm{f}} + k_{\mathrm{r}}/e_{\mathrm{r}})$ is the elastic load transfer load, a function of the roll stiffness.

The lateral acceleration a_y used in Equations (3) and (4) is generated at the cog. The accelerometer, however, is unable to distinguish between the acceleration caused by the vehicle's motion on the one hand, and the gravitational acceleration on the other. In fact the signal a_{ym}, sensed by the lateral accelerometer, is a combination of the gravitational force and the acceleration of the vehicle as represented in the following equation (case of small roll angle):

$$a_{ym} = a_y + g\theta. \tag{5}$$

Measuring the roll angle requires additional sensors, which makes it a difficult and costly operation. In this study, we consider that the roll angle can be calculated via relative suspension sensors. During cornering on a smooth road, the suspension is compressed on the outside and extended on the inside of the vehicle. If we neglect pitch dynamic effects on roll motion, the roll angle can be calculated by applying the following equation based on the geometry of the

roll motion [12,13]:

$$\theta = \frac{(\delta_{\mathrm{fl}} - \delta_{\mathrm{fr}} + \delta_{\mathrm{rl}} - \delta_{\mathrm{rr}})}{(2e_{\mathrm{f}})} - \frac{m_{\mathrm{v}} a_{ym} h}{k_{\mathrm{t}}}, \tag{6}$$

where k_{t} is the roll stiffness resulting from tyre stiffness.

3.1. *Stochastic state–space representation-observer* $O_{1\mathrm{L}}$

By combining the relations (3)–(6), the stochastic state–space representation of the model described in the previous section can be given as follows:

$$\begin{cases} \dot{X}(t) &= AX(t) + b_m(t) \\ Z(t) &= HX(t) + b_{\mathrm{s}}(t). \end{cases} \tag{7}$$

The state vector X is

$$X = \left[\Delta Fz_{\mathrm{l}} \Delta Fz_{\mathrm{r}}\ a_y\ \dot{a_y}\ \theta \dot{\theta}\right]. \tag{8}$$

It is initialised as a null vector. We assume that $\dot{a_y}$ is represented using a nondescriptive model ($\dot{\dot{a_y}} = 0$).

The observation vector Z is

$$Z = \left[a_{ym}(\Delta Fz_{\mathrm{l}} + \Delta Fz_{\mathrm{r}})\theta \dot{\theta} \Delta Fz_{\mathrm{l}}\right], \tag{9}$$

where

- a_{ym}, lateral acceleration measured by the accelerometer;
- $\Delta Fz_l + \Delta Fz_r$, the sum of right and left transfer loads is assumed to be zero at each instant;
- θ, roll angle calculated using Equation (6);
- $\dot{\theta}$, roll rate measured directly by the gyrometer; and
- ΔFz_l, left transfer load calculated from Equation (4).

The process and measurement noise vectors, respectively, $b_m(t)$ and $b_s(t)$, are assumed to be white, zero mean and uncorrelated. The constant matrices A and h are given as:

$$A = \begin{pmatrix} 0 & 0 & 0 & -2\dfrac{m_{\mathrm{s}}}{l}\left(\dfrac{l_{\mathrm{r}}h_{\mathrm{f}}}{e_{\mathrm{f}}} + \dfrac{l_{\mathrm{f}}h_{\mathrm{r}}}{e_{\mathrm{r}}}\right) & 0 & -2\left(\dfrac{k_{\mathrm{f}}}{e_{\mathrm{f}}} + \dfrac{k_{\mathrm{r}}}{e_{\mathrm{r}}}\right) \\ 0 & 0 & 0 & 2\dfrac{m_{\mathrm{s}}}{l}\left(\dfrac{l_{\mathrm{r}}h_{\mathrm{f}}}{e_{\mathrm{f}}} + \dfrac{l_{\mathrm{f}}h_{\mathrm{r}}}{e_{\mathrm{r}}}\right) & 0 & 2\left(\dfrac{k_{\mathrm{f}}}{e_{\mathrm{f}}} + \dfrac{k_{\mathrm{r}}}{e_{\mathrm{r}}}\right) \\ 0 & 0 & 0 & 1 & 0 & 0 \\ 0 & 0 & 0 & 0 & 0 & 0 \\ 0 & 0 & 0 & 0 & 0 & 1 \\ 0 & 0 & m_{\mathrm{s}}\dfrac{h_{\mathrm{cr}}}{I_{xx}} & 0 & \dfrac{m_{\mathrm{s}}gh_{\mathrm{cr}} - K_{\mathrm{R}}}{I_{xx}} & \dfrac{-C_{\mathrm{R}}}{I_{xx}} \end{pmatrix},$$

$$H = \begin{pmatrix} 0 & 0 & 1 & 0 & g & 0 \\ 1 & 1 & 0 & 0 & 0 & 0 \\ 0 & 0 & 0 & 0 & 1 & 0 \\ 0 & 0 & 0 & 0 & 0 & 1 \\ 1 & 0 & 0 & 0 & 0 & 0 \end{pmatrix}.$$

The state vector $X(t)$ will be estimated by applying a linear Kalman filter (LKF). The LKF is presented in Section 5.

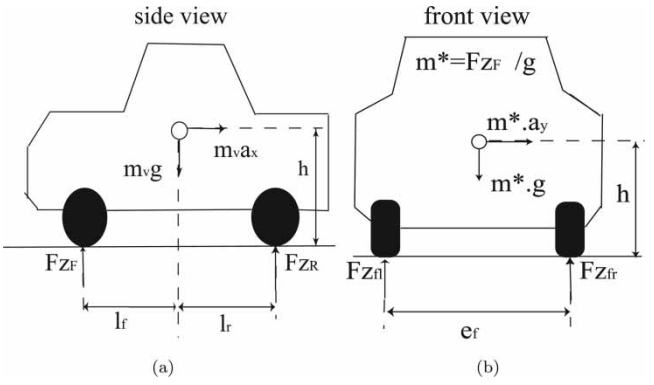

Figure 5. Load shifting (acceleration + cornering).

4. Block 3: wheel–ground vertical contact force models

As a result of longitudinal and lateral accelerations, the load distribution in a vehicle can significantly vary during a journey. It can be expressed by the vertical forces that act on each of the four wheels (see Figure 5). This section presents two models for calculating vertical forces. The first is a nonlinear model that takes into account longitudinal and lateral acceleration coupling, while the second applies the superposition assumption.

4.1. *Nonlinear model*

In this section a vertical force model will be discussed taking into account longitudinal and lateral acceleration coupling [7]. Constructing the torque balance at the rear axis contact point yields

$$lFz_{\mathrm{F}} = l_{\mathrm{r}} m_{\mathrm{v}} g - m_{\mathrm{v}} h a_x, \tag{10}$$

where a_x the longitudinal acceleration and Fz_{F} the vertical load on the front tyres. Consequently,

$$Fz_{\mathrm{F}} = m_{\mathrm{v}} \left(\frac{l_{\mathrm{r}}}{l} g - \frac{h}{l} a_x \right). \tag{11}$$

In addition, during cornering the lateral acceleration causes a roll torque that increases the load on the outside and decreases it on the inside of the vehicle.

The two axles are considered to be decoupled from one another. In the case of the front axle load a virtual mass m^* is used:

$$m^* = \frac{Fz_{\mathrm{F}}}{g}. \tag{12}$$

From the torque balance equation at the ground contact point of the front left wheel

$$Fz_{\mathrm{fr}} e_{\mathrm{f}} = Fz_{\mathrm{F}} \frac{e_{\mathrm{f}}}{2} + m^* a_y h, \tag{13}$$

where Fz_{ij} is the vertical load on each wheel. Solving for Fz_{fr}, and by analogy for the other forces, these can be formulated as follows:

$$\begin{cases} Fz_{\mathrm{fl}} = \dfrac{1}{2}m_{\mathrm{v}}\left(\dfrac{l_{\mathrm{r}}}{l}g - \dfrac{h}{l}a_x\right) - m_{\mathrm{v}}\left(\dfrac{l_{\mathrm{r}}}{l}g - \dfrac{h}{l}a_x\right)\dfrac{h}{e_{\mathrm{f}}g}a_y \\ Fz_{\mathrm{fr}} = \dfrac{1}{2}m_{\mathrm{v}}\left(\dfrac{l_{\mathrm{r}}}{l}g - \dfrac{h}{l}a_x\right) + m_{\mathrm{v}}\left(\dfrac{l_{\mathrm{r}}}{l}g - \dfrac{h}{l}a_x\right)\dfrac{h}{e_{\mathrm{f}}g}a_y \\ Fz_{\mathrm{rl}} = \dfrac{1}{2}m_{\mathrm{v}}\left(\dfrac{l_{\mathrm{f}}}{l}g + \dfrac{h}{l}a_x\right) - m_{\mathrm{v}}\left(\dfrac{l_{\mathrm{f}}}{l}g + \dfrac{h}{l}a_x\right)\dfrac{h}{e_{\mathrm{r}}g}a_y \\ Fz_{\mathrm{rr}} = \dfrac{1}{2}m_{\mathrm{v}}\left(\dfrac{l_{\mathrm{f}}}{l}g + \dfrac{h}{l}a_x\right) + m_{\mathrm{v}}\left(\dfrac{l_{\mathrm{f}}}{l}g + \dfrac{h}{l}a_x\right)\dfrac{h}{e_{\mathrm{r}}g}a_y. \end{cases} \tag{14}$$

4.1.1. *Stochastic state–space representation-observer* $O_{2\mathrm{N}}$

Using relations (14) and the estimated results from the second block, a nonlinear state–space representation (nonlinear evolution model and linear observation model) of the system described in the section above is given as:

$$\begin{cases} \dot{X}(t) = f(X(t)) + b_m(t) \\ Z(t) = h(X(t)) + b_{\mathrm{s}}(t). \end{cases} \tag{15}$$

The vehicle state vector X is

$$X = \begin{bmatrix} Fz_{\mathrm{fl}} & Fz_{\mathrm{fr}} & Fz_{\mathrm{rl}} & Fz_{\mathrm{rr}} & a_x & \dot{a}_x & a_y & \dot{a}_y \end{bmatrix}. \tag{16}$$

It is initialised as follows:

$$X_0 = [m_{\mathrm{fl}}g \quad m_{\mathrm{fr}}g \quad m_{\mathrm{rl}}g \quad m_{\mathrm{rr}}g \quad 0 \quad 0 \quad 0 \quad 0]. \tag{17}$$

The particular nonlinear functions of the state equation are then given by:

$$\begin{cases} f_1 = \dfrac{-h}{2l}m_{\mathrm{v}}x_6 - m_{\mathrm{v}}\dfrac{l_{\mathrm{r}}h}{le_{\mathrm{f}}}x_8 + m_{\mathrm{v}}\dfrac{h^2}{le_{\mathrm{f}}g}x_5x_8 + m_{\mathrm{v}}\dfrac{h^2}{le_{\mathrm{f}}g}x_6x_7 \\ f_2 = \dfrac{-h}{2l}m_{\mathrm{v}}x_6 + m_{\mathrm{v}}\dfrac{l_{\mathrm{r}}h}{le_{\mathrm{f}}}x_8 - m_{\mathrm{v}}\dfrac{h^2}{le_{\mathrm{f}}g}x_5x_8 - m_{\mathrm{v}}\dfrac{h^2}{le_{\mathrm{f}}g}x_6x_7 \\ f_3 = \dfrac{h}{2l}m_{\mathrm{v}}x_6 - m_{\mathrm{v}}\dfrac{l_{\mathrm{f}}h}{le_{\mathrm{r}}}x_8 - m_{\mathrm{v}}\dfrac{h^2}{le_{\mathrm{r}}g}x_5x_8 - m_{\mathrm{v}}\dfrac{h^2}{le_{\mathrm{r}}g}x_6x_7 \\ f_4 = \dfrac{h}{2l}m_{\mathrm{v}}x_6 + m_{\mathrm{v}}\dfrac{l_{\mathrm{f}}h}{le_{\mathrm{r}}}x_8 + m_{\mathrm{v}}\dfrac{h^2}{le_{\mathrm{r}}g}x_5x_8 + m_{\mathrm{v}}\dfrac{h^2}{le_{\mathrm{r}}g}x_6x_7 \\ f_5 = x_6 \\ f_6 = 0 \\ f_7 = x_8 \\ f_8 = 0. \end{cases} \tag{18}$$

The measurement vector Z,

$$Z = \begin{bmatrix} \Delta F z_{\mathrm{l}} & (F z_{\mathrm{fl}} + F z_{\mathrm{fr}}) & a_x & a_y & \sum F_{ij} \end{bmatrix} \tag{19}$$

consists of the following measurements:

- $\Delta F z_{\mathrm{l}}$ is provided by the second block;
- $F z_{\mathrm{fl}} + F z_{\mathrm{fr}}$ is calculated directly from Equation (14);
- a_x is measured using an accelerometer;
- a_y is provided by the second block; and
- $\sum F_{ij}$ is assumed to be equal to $m_{\mathrm{v}} g$ at each instant.

The observation functions take the form:

$$\begin{cases} h_1 = x_1 - x_2 + x_3 - x_4 \\ h_2 = x_1 + x_2 \\ h_3 = x_5 \\ h_4 = x_7 \\ h_5 = x_1 + x_2 + x_3 + x_4. \end{cases} \tag{20}$$

The state vector $X(t)$ will be estimated by applying an extended Kalman filter (EKF). The EKF is presented in Section 5.

4.2. *Linear model*

In this section a linear model that assumes the principle of superposition is used for calculating vertical forces [5]. The principle of superposition states that the total of a series of effects considered concurrently is identical to the sum of the individual effects considered individually. Therefore, we can numerically add the changes in wheel loads resulting from lateral and longitudinal load transfer in order to produce loads that are valid for combined operational conditions.

As proved in the previous section, and without taking into account the coupling term ($m^* = m_{\mathrm{v}} l_{\mathrm{r}} / l$), the vertical forces are given as:

$$\begin{cases} F z_{\mathrm{fl}} = m_{\mathrm{v}} g \dfrac{l_{\mathrm{r}}}{2l} - m_{\mathrm{v}} \dfrac{h}{2l} a_x - m_{\mathrm{v}} \dfrac{h l_{\mathrm{r}}}{e_{\mathrm{f}} l} a_y \\ F z_{\mathrm{fr}} = m_{\mathrm{v}} g \dfrac{l_{\mathrm{r}}}{2l} - m_{\mathrm{v}} \dfrac{h}{2l} a_x + m_{\mathrm{v}} \dfrac{h l_{\mathrm{r}}}{e_{\mathrm{f}} l} a_y \\ F z_{\mathrm{rl}} = m_{\mathrm{v}} g \dfrac{l_{\mathrm{f}}}{2l} + m_{\mathrm{v}} \dfrac{h}{2l} a_x - m_{\mathrm{v}} \dfrac{h l_{\mathrm{f}}}{e_{\mathrm{r}} l} a_y \\ F z_{\mathrm{rr}} = m_{\mathrm{v}} g \dfrac{l_{\mathrm{f}}}{2l} + m_{\mathrm{v}} \dfrac{h}{2l} a_x + m_{\mathrm{v}} \dfrac{h l_{\mathrm{f}}}{e_{\mathrm{r}} l} a_y. \end{cases} \tag{21}$$

4.2.1. *Stochastic state–space representation-observer O_{2L}*

Considering Equation (21) instead of Equation (14), the system described in Section 4.1.1 becomes linear. The evolution and observation matrices, respectively, A and H, are given as:

$$A = \begin{pmatrix} 0 & 0 & 0 & 0 & 0 & \frac{-m_v h}{2l} & 0 & \frac{-l_2 m_v h}{l e_1} \\ 0 & 0 & 0 & 0 & 0 & \frac{-m_v h}{2l} & 0 & \frac{l_2 m_v h}{l e_1} \\ 0 & 0 & 0 & 0 & 0 & \frac{m_v h}{2l} & 0 & \frac{-l_1 m_v h}{l e_2} \\ 0 & 0 & 0 & 0 & 0 & \frac{m_v h}{2l} & 0 & \frac{l_1 m_v h}{l e_2} \\ 0 & 0 & 0 & 0 & 0 & 1 & 0 & 0 \\ 0 & 0 & 0 & 0 & 0 & 0 & 0 & 0 \\ 0 & 0 & 0 & 0 & 0 & 0 & 0 & 1 \\ 0 & 0 & 0 & 0 & 0 & 0 & 0 & 0 \end{pmatrix},$$

$$H = \begin{pmatrix} 1 & -1 & 1 & -1 & 0 & 0 & 0 & 0 \\ 1 & 1 & 0 & 0 & 0 & 0 & 0 & 0 \\ 0 & 0 & 0 & 0 & 1 & 0 & 0 & 0 \\ 0 & 0 & 0 & 0 & 0 & 0 & 1 & 0 \\ 1 & 1 & 1 & 1 & 0 & 0 & 0 & 0 \end{pmatrix}.$$

The state vector $X(t)$ will be estimated by applying the LKF.

5. Estimation methods

In order to estimate the lateral load transfer and vertical tyre forces presented in Section 4, an observer-based approach is needed. This section introduces the estimation concept and presents the Kalman filter algorithm.

A simple example of an open-loop observer is the model given by relations (4), (6) and (14). Because of the system–model mismatch (unmodelled dynamics, parameter variations, ...) and the presence of unknown, unmeasurable disturbances, the estimates obtained from the open-loop observer would deviate from the actual values over time. In order to reduce the estimation error, at least some of the measured outputs are compared with the same variables estimated by the observer. The difference is fed back into the observer after being multiplied by a gain matrix K, and so we have a closed-loop observer [12]. A schematic block diagram for our observers is given in Figure 6. All observers were implemented in a first-order Euler approximation discrete form. At each iteration, the state vector is first calculated according to the evolution equation and then corrected online with measurement errors (innovation) and filter gain K in a prediction–correction recursive mechanism. The gain is calculated by the Kalman filter method.

5.1. *Structure of the estimation concept*

The Kalman filter is essentially a set of mathematical equations that implement a predictor–corrector type estimator [14–16]. It is optimal in the sense that it minimises the estimated

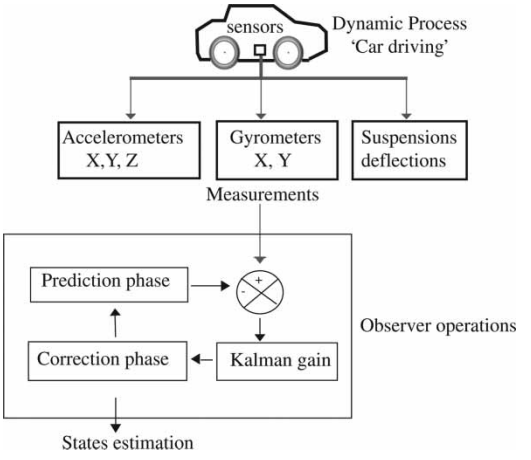

Figure 6. Observer operations.

error covariance under certain given assumptions. The stochastic discrete form of state–space models presented in the preceding sections is

$$\begin{aligned} X_{k+1} &= f(X_k, u_k, b_{m,k}) \\ Z_k &= h(X_k, b_{s,k}), \end{aligned} \tag{22}$$

where $b_{m,k}$ and $b_{s,k}$ represent model and measurement noise at time t_k, and u_k is the system input.

Assuming that noises are Gaussian, white and centred, with Q_k and R_k the noise variance–covariance matrices for $b_{m,k}$ and $b_{s,k}$, respectively, and $f()$ and $h()$ linear functions, these constraints reduce the state-model:

$$\begin{cases} X_{k+1} &= A_k X_k + B_k u_k + b_{m,k} \\ Z_k &= H_k X_k + b_{s,k}. \end{cases} \tag{23}$$

Given that our observers have no inputs ($u_k = 0$), and with $\widehat{X}_{k/k-1}$ and $\widehat{X}_{k/k}$ the state prediction and estimation vectors, respectively, at time t_k, the LKF requires the following equations:

Predict next state, before measurements are taken:

$$\begin{aligned} \widehat{X}_{k/k-1} &= A_k \widehat{X}_{k-1/k-1} \\ P_{k/k-1} &= A_k P_{k-1/k-1} A_k^t + Q_k. \end{aligned} \tag{24}$$

Update state, after measurements are taken:

$$\begin{aligned} K_k &= P_{k/k-1} H_k^t (H_k P_{k/k-1} H_k^t + R_k)^{-1} \\ \widehat{X}_{k/k} &= \widehat{X}_{k/k-1} + K_k (z_k - H_k \widehat{X}_{k/k-1}) \\ P_{k/k} &= (I - K_k H_k) P_{k/k-1}, \end{aligned} \tag{25}$$

where K is the Kalman gain used in the update data, and P the covariance matrix for the state estimate containing information about the accuracy of the data. The EKF works almost like a regular Kalman filter, except that it linearises the system before the estimation, by calculating

the Jacobian (matrix of all partial derivatives of a vector) of the nonlinear equations around the estimated states:

$$A_k = \frac{\partial f(\widehat{X}_{k/k}, u_k, 0)}{\partial X}$$
$$H_k = \frac{\partial f(\widehat{X}_{k/k-1}, 0)}{\partial X}. \tag{26}$$

6. Observability analysis

Observability is a measure of how well the internal states of a system can be inferred by knowledge of its inputs and external outputs.

6.1. *Linear system*

The systems described in Sections 3.1 and 4.2.1 are observable. We have verified that the observability matrix O, defined in Equation (27), for each system has full rank:

$$O = \begin{bmatrix} C & CA & CA^2 \cdots CA^{n-1} \end{bmatrix}, \tag{27}$$

where n represents state–space vector dimension.

6.2. *Nonlinear system*

Using the nonlinear state–space formulation of the system described in Section 4.1.1, the observability definition is local and uses the Lie derivative [17]. The Lie derivative of h_i function, at $p+1$ order, is defined as

$$L_{\mathrm{f}}^{p+1} h_i(X) = \frac{\partial L_{\mathrm{f}}^{p} h_i(X)}{\partial X} f(X, u) \tag{28}$$

with

$$L_{\mathrm{f}}^{1} h_i(X) = \frac{\partial h_i(X)}{\partial X} f(X, u). \tag{29}$$

The observability function o_i corresponding to the measurement function h_i is defined as

$$o_i = \begin{pmatrix} \mathrm{d}h_i(X) \\ \mathrm{d}L_{\mathrm{f}}^{1} h_i X) \\ \cdots \\ \mathrm{d}L_{\mathrm{f}}^{7} h_i(X) \end{pmatrix}. \tag{30}$$

where d is the operator:

$$\mathrm{d}h_i = \left(\frac{\partial h_i}{\partial x_1}, \ldots, \frac{\partial h_i}{\partial x_8} \right). \tag{31}$$

The observability function of the system is calculated as

$$O = \begin{pmatrix} o_1 \\ \cdots \\ o_5 \end{pmatrix}. \tag{32}$$

The ranks of all observability functions, calculated along experimental trajectories, corresponded to the state vector dimensions, and so the system described in Section 4.1.1 is

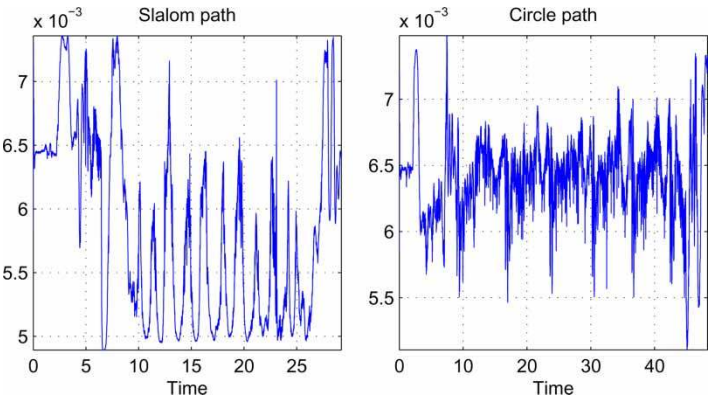

Figure 7. Observability index parameter for the slalom and circle trajectories.

locally observable. The standard definition of observability for linear systems with unchanged parameter is a 'yes' or 'no' measure; that is, the system is either observable or not. For non-linear systems, it seems reasonable to suppose that there are regions in phase space that are less observable than others. In order to quantify system observability degree, we use an observability index, defined as

$$\Lambda(x) = \frac{\lambda_{\min}[O^{\mathrm{T}}O, x(t)]}{\lambda_{\max}[O^{\mathrm{T}}O, x(t)]}, \tag{33}$$

where $\lambda_{\max}[O^{\mathrm{T}}O, x(t)]$ indicates the maximum eigen value of matrix $O^{\mathrm{T}}O$ estimated at point $x(t)$ (likewise for $\lambda_{\min}$). Then, $0 \leq \Lambda(x) \leq 1$, and the lower bound is reached when the system is unobservable at point x ([18,19]). The index defined in Equation (33) is a type of condition number of the observability matrix O. Figure 7 presents index parameter of matrix O for the manoeuvre computed using data acquired from a moving vehicle in experimental tests (see Section 9).

7. LTR calculation

In this section we indicate the importance of online measurement of the tyre loads in rollover vehicle prediction and rollover controller design.

The rollover index LTR, which is simply represented in Equation (34), is suggested as a convenient method for supervising the vehicle's dynamic roll behaviour [4],

$$\mathrm{LTR} = \frac{Fz_{\mathrm{l}} - Fz_{\mathrm{r}}}{Fz_{\mathrm{l}} + Fz_{\mathrm{r}}} = \frac{\Delta Fz_{\mathrm{l}}}{Fz_{\mathrm{l}} + Fz_{\mathrm{r}}}, \tag{34}$$

where Fz_{l} and Fz_{r} are, respectively, vertical loads on the left and right tyres. The value of LTR varies from -1 at the lift-off of the left wheel, tends toward 0 at no load transfer and to 1 at the lift-off of the right wheel. A simplified steady-state approximation of LTR in terms of lateral acceleration a_{ym} and the cog height h is given as [20]:

$$\mathrm{LTR} = 2\frac{a_{ym}h}{ge_m}, \tag{35}$$

where a_{ym} is the lateral accelation and e_m is the width tracks average value ($e_m = (e_{\mathrm{f}} + e_r)/2$). One of this article's contributions is our observation that the rollover estimation based upon

Equation (35) is not sufficient to detect the rollover transient phase, and that the best way to identify the LTR is by estimating vertical forces. Subsequently, a precise direct measurement of the LTR can be used as a reliable rollover warning, or as a switch for a rollover controller [20].

Section 9 shows the LTR evaluation during experimental tests, while Section 9.4 illustrates the relation between the LTR and roll angle.

8. Effects of road angle

This section introduces briefly the effect of road angle on wheel–ground vertical force calculation. In fact, road disturbances such as road bank angle and road slope act directly on vehicle dynamics and accelerometer measurements, introducing significant effects on the normal force calculation. For example, accelerometer measurements are affected by the gravity component. Cancelling this component needs knowledge of road angle, which is a research topic in itself [21,22].

Consequently, knowing road angle values is a prerequisite for studying road disturbance effects on vehicle dynamics and measurements. However, dealing with these parameters is beyond the scope of this study.

Although this work neglected road angle when modelling, the estimation process is valid for small angles ($< 8\%$).

9. Experimental results and discussions

9.1. *Experimental car*

The experimental vehicle shown in Figure 8 is the INRETS-MA (Institut National de Recherche sur les Transports et leur Sécurité – Département Mécanismes d'Accidents) Laboratory's test vehicle. This Peugeot 307 is equipped with a number of sensors including accelerometers, gyrometers, steering angle sensors, linear relative suspension sensors and wheel force transducers that measure in real time the forces acting at the wheel centre. The sampling frequency of these sensors is 100 Hz.

Figure 8. Experimental vehicle.

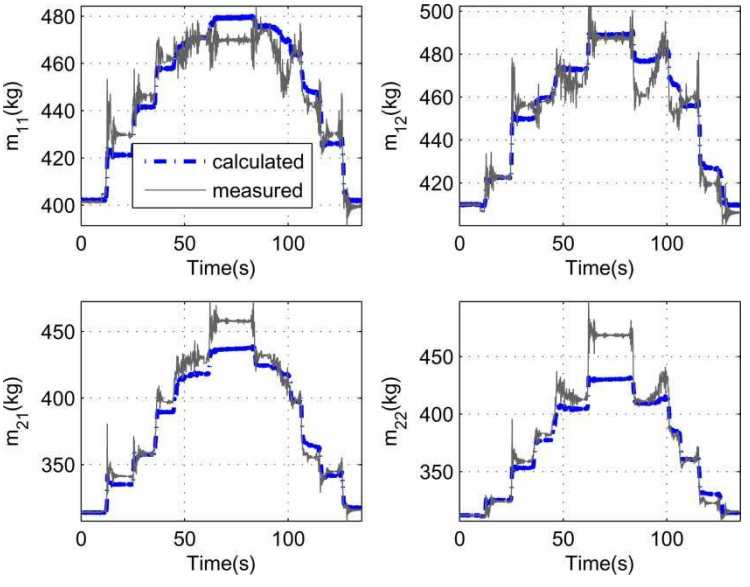

Figure 9. Load distribution in terms of number of passengers.

9.2. *Validation of the vehicle's weight identification method*

In order to validate the proposed vehicle's weight identification method (see Section 2), two experimental tests were done. Five passengers were asked to sit in the car. Measurements (vertical forces and suspension deflections) were done when at rest, when the car was empty, with one, then with two and so on until all five passengers were seated in the car. Measurements were then taken when these passengers left the car one after the other till it was empty again. By disregarding suspension dynamics, we suppose that real m_{ij} are equal to Fz_{ij}/g, where the Fz_{ij} are measured by the wheel force transducers. Figure 9 compares real m_{ij} and the identified ones (see Section 2). Although the identification method is simple, results are globally acceptable. However, some differences appear because of noises, model simplification and suspension deflection sensors precision. In the remainder, the identification method was applied in order to initialise the observers (see Section 4).

9.3. *Observers validation*

Test data from nominal as well as adverse driving conditions were used to assess the performance of observers in realistic driving situations. Among numerous experimental tests, two tests are presented: a 'starting–slalom–braking' and a circle. These tests are representative of both longitudinal and lateral dynamic behaviours. The vehicle trajectories, speeds and the acceleration diagrams of both tests are shown, respectively, in Figures 10 and 11. Acceleration diagrams show that large lateral accelerations were obtained (absolute value up to 0.5 g), meaning that the experimental vehicle was put in a critical driving situation.

The performance of the developed observers can be characterised by the normalised mean and normalised standard deviation (SD). The normalised error is defined in [19] as:

$$\epsilon_z = 100 \times \frac{\|z_{\text{obs}} - z_{\text{measured}}\|}{\max(\|z_{\text{measured}}\|)}, \tag{36}$$

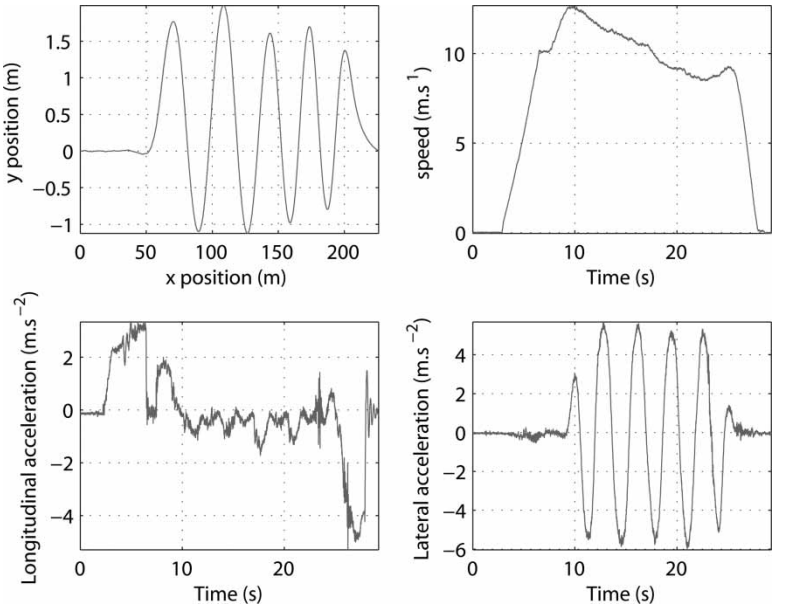

Figure 10. Experimental test: vehicle positions, speed and acceleration diagrams for the slalom test.

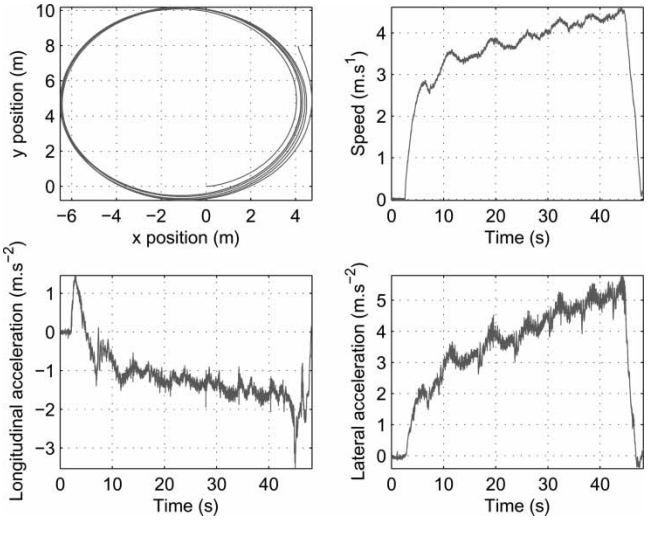

Figure 11. Experimental test: vehicle positions, speed and acceleration diagrams for the circle test.

where z_{obs} is the variable calculated by the observer, z_{measured} is the measured variable and $\max(\|z_{\text{measured}}\|)$ is the absolute maximum value of the measured variable during the test manoeuvre.

9.3.1. *Slalom test*

During the slalom test (see Figure 10), the vehicle first accelerated up to $a_x \approx 0.3$ g, then negotiated a slalom at a velocity of $10\,\text{ms}^{-1}$ with $-0.6\,\text{g} \leq a_y \leq 0.6\,\text{g}$, before finally decelerating

Table 1. Observer O_{1L}: maximum absolute values, normalised mean errors and normalised SD.

Slalom	Maximum ($\|\|\|$)	Mean (%)	SD (%)	Circle	Maximum ($\|\|\|$)	Mean (%)	SD (%)
ΔFz_l	7705 (N)	4.05	3.08	ΔFz_l	7088 (N)	3.40	3.01
θ	0.04 (rad)	2.75	2.67	θ	0.03 (rad)	4.83	0.74

Table 2. Observers O_{2L} and O_{2N}: maximum absolute values, normalised mean errors and normalised SD for the slalom test.

		Mean (%)		SD (%)	
	Maximum ($\|\|\|$)	O_{2L}	O_{2N}	O_{2L}	O_{2N}
Fz_{fl}	6386 (N)	2.42	2.35	2.30	2.38
Fz_{fr}	6958 (N)	2.01	2.06	1.94	1.99
Fz_{rl}	4906 (N)	2.38	3.97	2.60	4.51
Fz_{rr}	4862 (N)	1.99	3.78	2.22	4.36
LTR	0.53	3.97	3.97	4.60	4.61

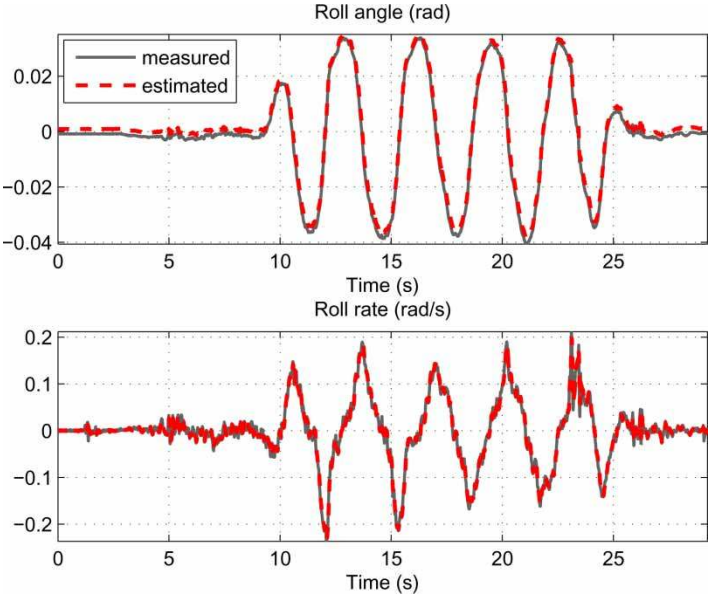

Figure 12. Roll angle and roll rate.

to $a_x \approx -0.5$ g. In the following, we propose to compare estimation results and the obtained real measures. Tables 1 and 2 present maximum absolute values, normalised mean errors and normalised SD for lateral transfer load, roll angle, vertical forces and the LTR parameter. Figure 12 presents the roll angle and the changes in the roll rate during the trajectory. Figure 13 shows the one-side lateral load transfer, while Figures 14 and 15 show vertical forces on the front and rear wheels. We can deduce that for this test the performance of the observer is satisfactory.

Finally, Figure 16 compares the LTR obtained from measured forces with the LTR obtained from estimated forces. We deduce that the estimated LTR fits the measured LTR well. Online calculation of the LTR is essential for rollover avoidance; when LTR exceeds a set value ($|LTR| > 0.6$), the driver must be alerted in order to prevent a dangerous situation.

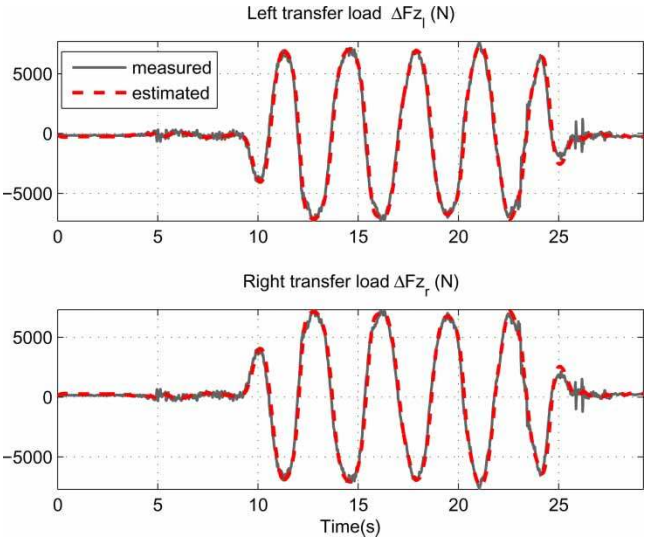

Figure 13. Lateral transfer load.

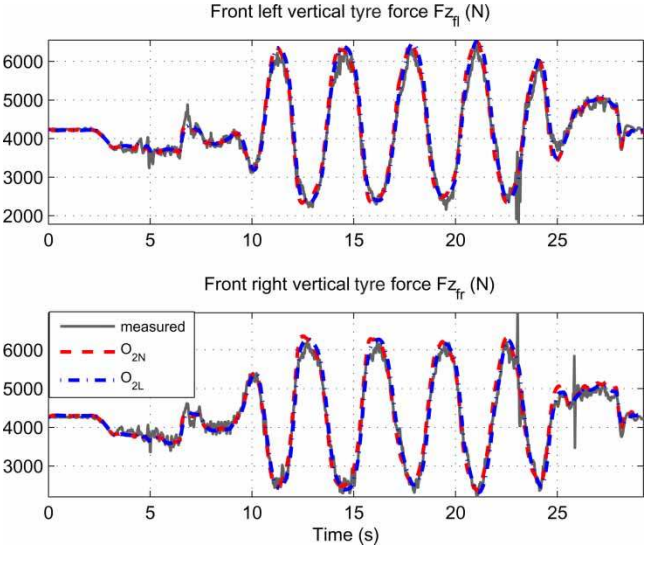

Figure 14. Estimation of front vertical tyre forces.

9.3.2. *Circle test*

In the second test the vehicle performed a circle on a random road profile at maximum steering angle of 40° (see Figure 11). Acceleration diagrams show that large lateral accelerations persist for more than 20 s. Tables 1 and 3 along with Figures 17–20 show that the estimation results are relatively good, although not as good as in the slalom test. The explanation is that in the circle test camber angles are high and change the shape of the contact patch, consequently influencing vehicle dynamics substantially. In addition, we believe this to be a result of road irregularities, which act on vertical suspension dynamics and influence vertical forces.

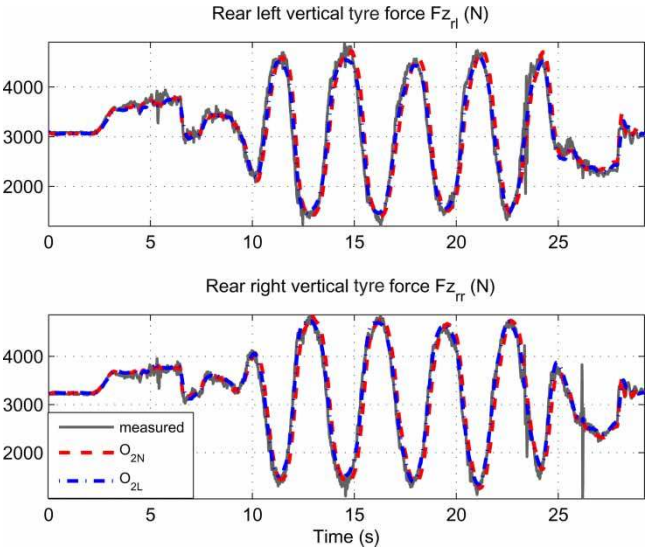

Figure 15. Estimation of rear vertical tyre forces.

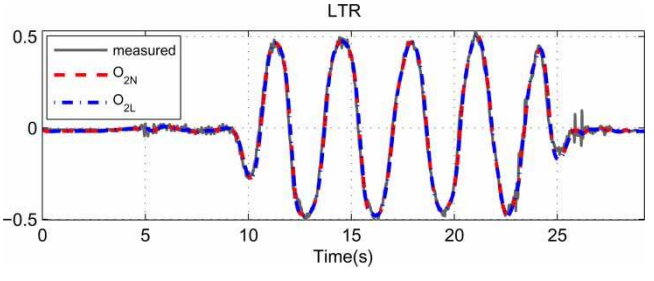

Figure 16. Estimation of the LTR parameter.

Table 3. Observers O_{2L} and O_{2N}: maximum absolute values, normalised mean errors and normalised SD for the circle test.

		Mean (%)		SD (%)	
	Maximum ($\|\|\|$)	O_{2L}	O_{2N}	O_{2L}	O_{2N}
Fz_{fl}	4788 (N)	3.62	3.54	2.74	2.65
Fz_{fr}	6889 (N)	4.99	3.65	3.12	2.49
Fz_{rl}	3438 (N)	5.31	5.21	3.46	3.42
Fz_{rr}	4876 (N)	5.79	4.10	3.15	2.58
LTR	0.48	3.20	3.18	2.87	2.86

The circle test shows robustness of the applied process. Indeed, although the experimental test violated some initial simplifying assumptions (road irregularities, suspension dynamics and high camber angle), the observers were able to function well.

9.4. *Comparison between linear and nonlinear observers: O_{2L} vs O_{2N}*

Comparing observers O_{2L} and O_{2N} from the experimental tests, we find that they give similar results for the slalom test, but not for the circle test. Heavily longitudinal and lateral dynamics

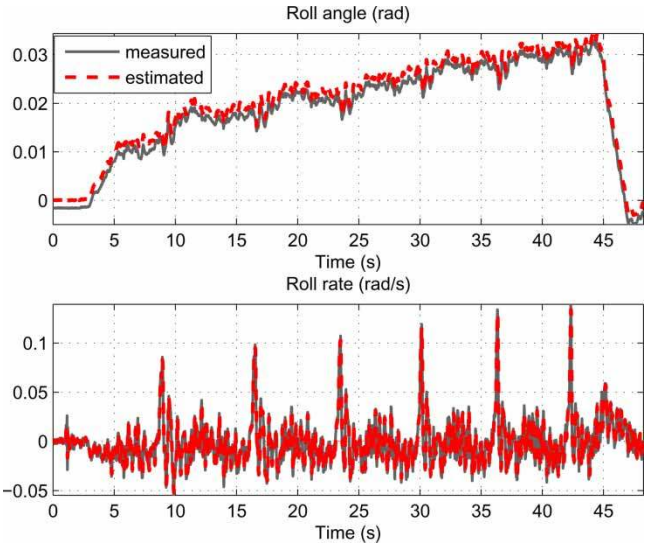

Figure 17. Roll angle and roll rate.

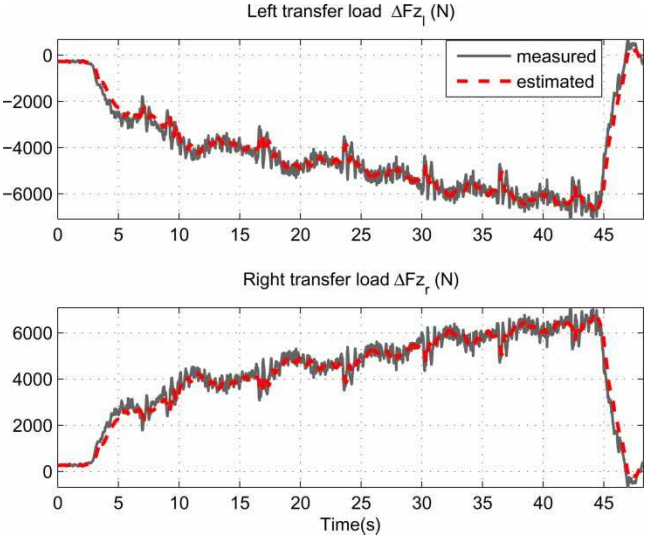

Figure 18. Lateral transfer load.

do not appear simultaneously in the slalom test. Therefore, the product $a_x a_y \to 0$, and the superposition principle are always valuable. Conversely, in the circle test, longitudinal and lateral coupling dynamics are significant, especially in traction on the front wheels to maintain the speed, and observer O_{2N} proves able to work better than O_{2L}.

9.5. *Relation between* LTR *and roll angle*

It will be of interest to illustrate the relation between the estimated LTR and the roll angle obtained according to the measurements of the suspension relative displacement sensors.

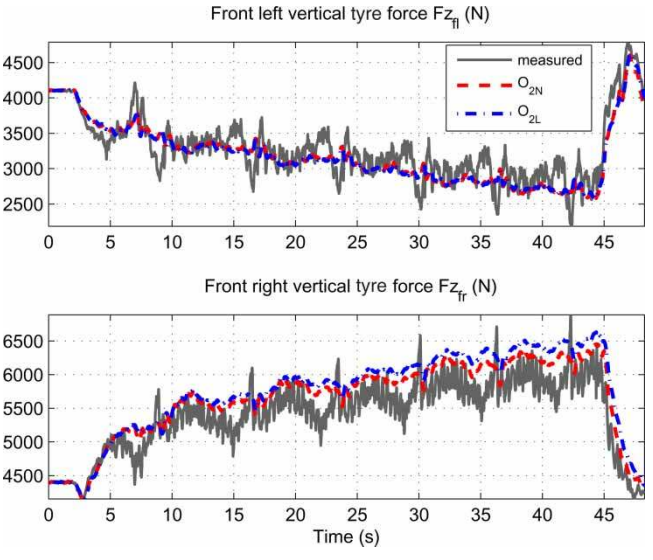

Figure 19. Estimation of front vertical tyre forces.

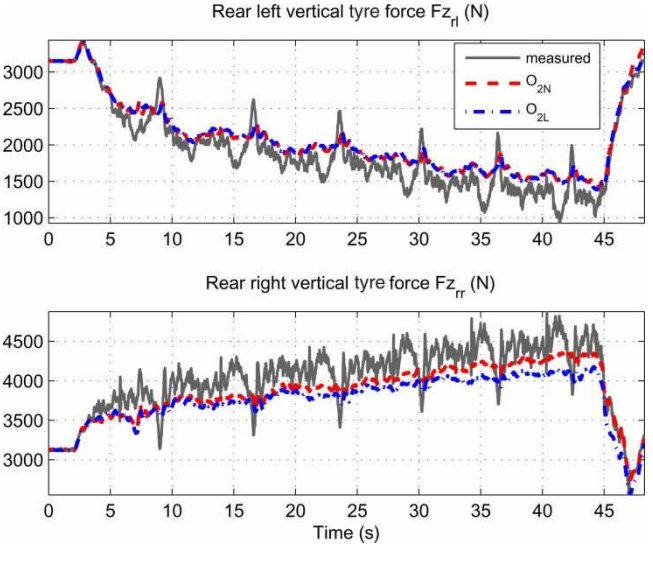

Figure 20. Estimation of rear vertical tyre forces.

Figure 21 shows a linear relationship between LTR and roll angle. This relationship becomes apparent when Equations (4) and (34) are combined. The linearity is valid as long as the suspension operates in linear mode, meaning that roll stiffness is constant. However, when roll angle greatly increases, nonlinear suspension behaviour occurs, causing the roll stiffness to increase gradually [23].

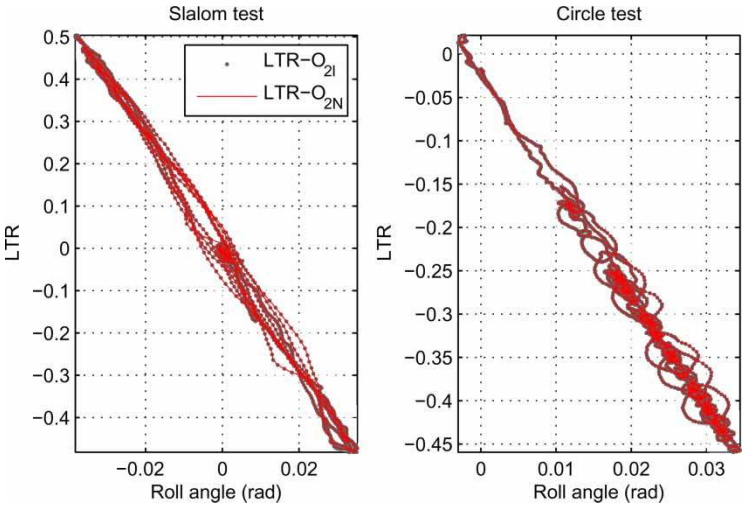

Figure 21. Relation between LTR and roll angle.

10. Conclusions and future works

This article has presented a new algorithm to estimate lateral transfer load and vertical tyre forces, regardless of the tyre model. Our study presents three observers (O_{1L}, O_{2L} and O_{2N}) developed for this purpose and based on the Kalman filter. Observer O_{1L} is based on a roll dynamics model and provides lateral load transfer estimation. Observers O_{2L} and O_{2N} are derived, respectively, from linear and nonlinear models. The linear model rests on the longitudinal and lateral dynamics superposition principle, while the nonlinear model proposes coupling these dynamics. The LTR rollover index parameter was also calculated and discussed within the context of estimating vertical wheel forces.

Experimental evaluations in real-time embedded estimation processes yield good estimations close to the measurements. However, we note that the observer O_{2N} gives better results when high longitudinal/lateral accelerations act simultaneously. The potential of the estimation process demonstrates that it may be possible to replace expensive dynamometric hub sensors by software observers that can work in real time while the vehicle is in motion. This is one of the important results of our work.

Although the identified mass tends towards the real mass value, one of the weak points of this approach is the determination of the vehicle's mass, which is highly dependent on the sensitivity of the relative suspension sensors. Moreover, the suspension model is considered linear, which does not always correspond to reality. Future studies will improve the vehicle mass identification method, and take into account road irregularities and road angle, which can significantly impact load transfer.

Acknowledgements

This work was supported by the national PREDIT-SARI-RADARR project.

References

[1] F. Aparicio, J. Paez, F. Moreno, F. Jiminez, and A. Lopez, *Discussion of a new adaptive speed control system incorporating the geometric characteristics of the roadway*, Int. J. Veh. Auton. Syst. 3(1) (2005), pp. 47–64.

[2] J. Stephant, A. Charara, and D. Meizel, *Evaluation of a sliding mode observer for vehicle sideslip angle*, Control Eng. Pract. 15 (2007), pp. 803–812.
[3] G. Baffet, A. Charara, D. Lechner, and D. Thomas, *Experimental evaluation of observers for tire-road forces, sideslip angle and wheel cornering stiffness*, Veh. Syst. Dyn. 46 (2008), pp. 501–520.
[4] R. Kamnik, F. Boettiger, and K. Hunt, *Roll dynamics and lateral load transfer estimation in articulated heavy freight vehicles*, Proc.Inst. Mech. Eng. D, J. Automob. Eng. 217(13) (2003), pp. 985–997.
[5] D. Lechner, 2002, *Analyse du comportement dynamique des vehicules routiers légess: Développement d'une méthodologie appliquée à la sécurité primaire*. PhD diss., Ecole Centrale de Lyon.
[6] T. Shim and C. Ghike, *Understanding the limitations of different vehicle models for roll dynamics studies*, Veh. Syst. Dyn. 45 (2007), pp. 191–216.
[7] U. Kiencke and L. Nielsen, *Automotive Control Systems*, Springer-Verlag, Berlin/Heidelberg/New York, 2000.
[8] T.A. Wenzel, K.J. Burnham, M.V. Blundell, and R.A. Williams, *Dual extended Kalman filter for vehicle state and parameter estimation*, Veh. Syst. Dyn. 44 (2006), pp. 153–171.
[9] A. Vahidi, A. Stefanopoulou, and H. Peng, *Recursive least squares with forgetting for online estimation of vehicle mass and road grade: Theory and experiments*, Veh. Syst. Dyn. 43 (2005), pp. 31–55.
[10] W.F. Milliken and D.L. Milliken, *Race Car Vehicle Dynamics*, Society of Automotive Engineers, Inc. USA, 1995.
[11] R.A. Anderson, *Using GPS for model based estimation of critical vehicle states*, Masters science thesis, Auburn University 2004.
[12] A. Hac, T. Brown, and J. Martens, *Detection of Vehicle Rollover*, SAE World Congress, Detroit, Michigan, 2004.
[13] N.V. Rao, *An approach to rollover stability in vehicles using suspension relative position sensors and lateral acceleration sensors*, Master science thesis, Texas A&M University., 2005.
[14] G. Welch and G. Bishop, *An introduction to the Kalman filter*, Course 8, Department of Computer Science, University of North Carolina, Chapel Hill, USA, 2001.
[15] H. Durrant-Whyte, *Multi sensor data fusion*, Australian centre for field robotics, University of Sydney, NSW 2006, 2001.
[16] R.E. Kalman, *A new approach to linear filtering and prediction problems*, Trans. ASME, J. Basic Eng. 82(D) (1960), pp. 35–45.
[17] H. Nijmeijer and A.J. van der Schaft, *Nonlinear Dynamical Control Systems*, Springer-Verlag, Berlin, 1990.
[18] L.A. Aguirre and C. Letellier, *Observability of multivariate differential embeddings*, J. Phys. A, Math. Gen. 38 (2005), pp. 6311–6326.
[19] J. Stéphant, A. Charara, and D. Meizel, *Evaluation of sliding mode observer for vehicle sideslip angle*, Control Eng. Pract. 15 (2006), pp. 803–812.
[20] D. Odenthal, T. Bunte, and J. Ackerman, *Nonlinear steering and breaking control for vehicle rollover avoidance*, European control conference, Karlsruhe, Germany, 1999.
[21] H.E. Tseng, *Dynamic estimation of road bank angle*, Veh. Syst. Dyn. 36 (2001), pp. 307–328.
[22] Y. Sebsadji, S. Glaser, S. Mammar, and J. Dakhlallah, *Road slope and vehicle dynamics estimation*, American Control Conference, Seattle, Washington, USA, 2008.
[23] A. Hac, *Influence of chassis characteristics on sustained roll, heave and yaw oscillations in dynamic rollover testing*, SAE World Congress, Detroit, Michigan, 2005.